AD-A083 333 SRI INTERNATIONAL MENLO PARK CA F/G 4/1
EFFECTS OF IMPULSIVE HEATING EVENTS ON F-REGION CHEMISTRY AND E--ETC(U)
JUL 79 J D KELLY DNA001-77-C-0082
UNCLASSIFIED DNA-5028T NL

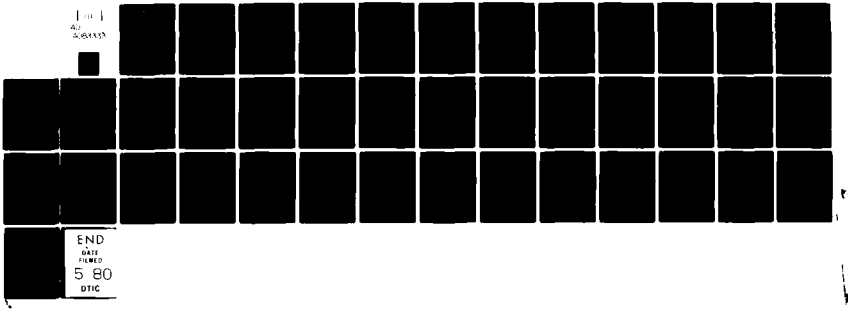

END
DATE FILMED
5 80
DTIC

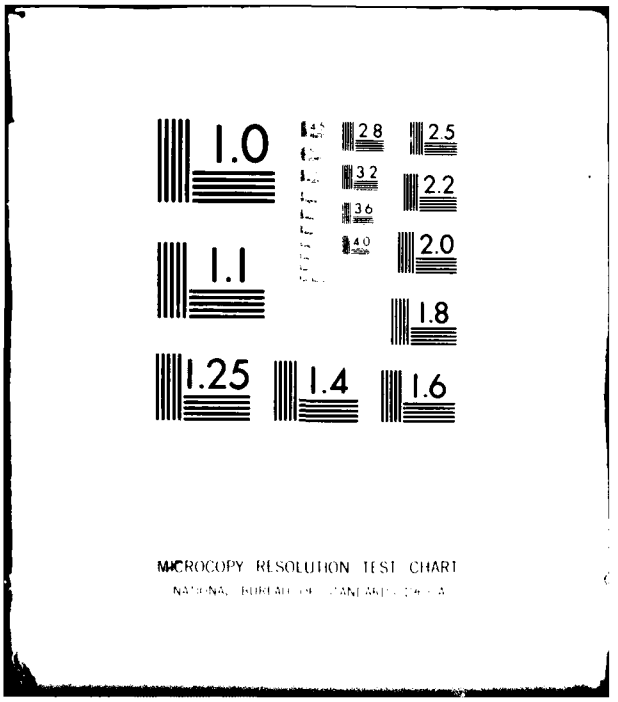
1.0
1.1
1.25
1.4
1.6
1.8
2.0
2.2
2.5
2.8
3.2
3.6
4.0
MICROCOPY RESOLUTION TEST CHART

(12) LEVEL III

DNA 5028T

EFFECTS OF IMPULSIVE HEATING EVENTS ON F-REGION CHEMISTRY AND ELECTRON DENSITY

HAES Report No. 81

John D. Kelly
SRI International
333 Ravenswood Avenue
Menlo Park, California 94025

31 July 1979

Topical Report for Period March 1978—July 1979

CONTRACT No. DNA 001-77-C-0042

THIS WORK SPONSORED BY THE DEFENSE NUCLEAR AGENCY
UNDER RDT&E RMSS CODE B322079462 I25AAXHX63132 H2590D.

Prepared for
Director
DEFENSE NUCLEAR AGENCY
Washington, D. C. 20305

Destroy this report when it is no longer needed. Do not return to sender.

PLEASE NOTIFY THE DEFENSE NUCLEAR AGENCY, ATTN: STTI, WASHINGTON, D.C. 20305, IF YOUR ADDRESS IS INCORRECT, IF YOU WISH TO BE DELETED FROM THE DISTRIBUTION LIST, OR IF THE ADDRESSEE IS NO LONGER EMPLOYED BY YOUR ORGANIZATION.

UNCLASSIFIED

SECURITY CLASSIFICATION OF THIS PAGE (When Data Entered)

REPORT DOCUMENTATION PAGE	READ INSTRUCTIONS BEFORE COMPLETING FORM
1. REPORT NUMBER: DNA 5028T	2. GOVT ACCESSION NO.: AD-A083 333
	3. RECIPIENT'S CATALOG NUMBER:
4. TITLE (and Subtitle): EFFECTS OF IMPULSIVE HEATING EVENTS ON F-REGION CHEMISTRY AND ELECTRON DENSITY HAES Report No. 81	5. TYPE OF REPORT & PERIOD COVERED: Topical Report for Period March 1978—July 1979
	6. PERFORMING ORG. REPORT NUMBER: SRI Project 5915
7. AUTHOR(s): John D. Kelly	8. CONTRACT OR GRANT NUMBER(s): DNA 001-77-C-0042 new
9. PERFORMING ORGANIZATION NAME AND ADDRESS: SRI International, 333 Ravenswood Avenue, Menlo Park, California 94025	10. PROGRAM ELEMENT, PROJECT, TASK AREA & WORK UNIT NUMBERS: Subtask I25AAXHX631-32
11. CONTROLLING OFFICE NAME AND ADDRESS: Director, Defense Nuclear Agency, Washington, D.C. 20305	12. REPORT DATE: 31 July 1979
	13. NUMBER OF PAGES: 42
14. MONITORING AGENCY NAME & ADDRESS(if different from Controlling Office)	15. SECURITY CLASS (of this report): UNCLASSIFIED
	15a. DECLASSIFICATION DOWNGRADING SCHEDULE

16. DISTRIBUTION STATEMENT (of this Report)

Approved for public release; distribution unlimited.

17. DISTRIBUTION STATEMENT (of the abstract entered in Block 20, if different from Report)

18. SUPPLEMENTARY NOTES

This work sponsored by the Defense Nuclear Agency under RDT&E RMSS Code B322079462 I25AAXHX63132 H2590D.

19. KEY WORDS (Continue on reverse side if necessary and identify by block number)

Atmospheric Heave
Joule Heat
Nuclear Effects

20. ABSTRACT (Continue on reverse side if necessary and identify by block number)

The Chatanika incoherent-scatter radar (located near Fairbanks, Alaska, L = 5.6) has been used to study the ionospheric effects of impulsive auroral heating events. In some cases, the time-integrated auroral energy deposition is similar in magnitude to that expected from a high altitude nuclear event outside the fireball region. The resulting ionospheric effects are significant. The elevated temperatures and atmospheric heave contribute to a substantial change in F-region ion chemistry, changing

DD FORM 1 JAN 73 1473 EDITION OF 1 NOV 65 IS OBSOLETE

UNCLASSIFIED

SECURITY CLASSIFICATION OF THIS PAGE (When Data Entered)

20. ABSTRACT (Continued)

the dominant F-region ion from atomic to molecular species. As a result, a significant depletion of the F-region electron density occurs. Currently, these effects are not accurately predicted by the nuclear codes, as the function of the codes is to predict the large-scale perturbations. The Chatanika radar data can be used to improve the ambient ionospheric models and to improve the predictions of F-region changes resulting from sudden heating events.

CONTENTS

LIST OF ILLUSTRATIONS

LIST OF TABLES

I INTRODUCTION

There has been substantial effort to model, and subsequently predict, the ionospheric effects of nuclear explosions at high altitudes. The effects which will have serious impact on both satellite and ground-based communications include sudden enhancement of electron density, and sudden heating of both neutral and charged species resulting in atmospheric heave.

Large electric fields of magnetospheric origin have substantial influence on the state of the ionosphere. These electric fields, through the process of joule heating, produce dramatic increases in the ion and neutral temperatures. In some instances the heating is sudden, and results in an upwelling or heave of the neutral atmosphere. This results in a change in ion chemistry, so that a depletion of electron density occurs.

Impulsive heating events have been observed by the Chatanika incoherent scatter radar (Chatanika, Alaska). Increases in ion temperatures of a few thousand degrees kelvin occur. Whether the heat source is a distant nuclear explosion or a large joule heating event, the resulting ionospheric modification should be similar. However, we find that the nuclear effects code, WEPH VI for example, does not predict similar effects. In fact, given sufficient time following a nuclear "event" the code never returns all of the parameters to ambient values.

The intent of the code is to predict only large scale perturbations. As a result, the less dramatic, but still significant, effects of heating the ionosphere outside of the fireball are generally ignored. These effects, though, affect a large volume of ionosphere changing the ion chemistry, and thus result in sufficient ionosphere depletion to limit HF propagation.

As the Chatanika radar can continuously measure ionospheric parameters before, during, and after impulsive joule heating events, the data should be very useful to improve the predictions made by nuclear effects codes.

II BACKGROUND

The high-latitude thermosphere, in contrast with the midlatitude thermosphere, is strongly coupled to the magnetosphere. As a result, large amounts of energy and momentum are transferred from the magnetosphere to the ionosphere. These energy inputs have a significant effect on the morphology, thermodynamics, and chemistry of the high-latitude ionosphere. In some cases, the magnitude of the energy deposition is similar to that of a distant nuclear explosion, i.e., the temperature enhancements are similar to those expected from nuclear sources. Energetic auroral particles are responsible for both heating effects and the production of ionization. Electric fields are responsible for joule heating. The relationship between the auroral processes and their manifestation in the high-latitude ionosphere is outlined in Figure 1.

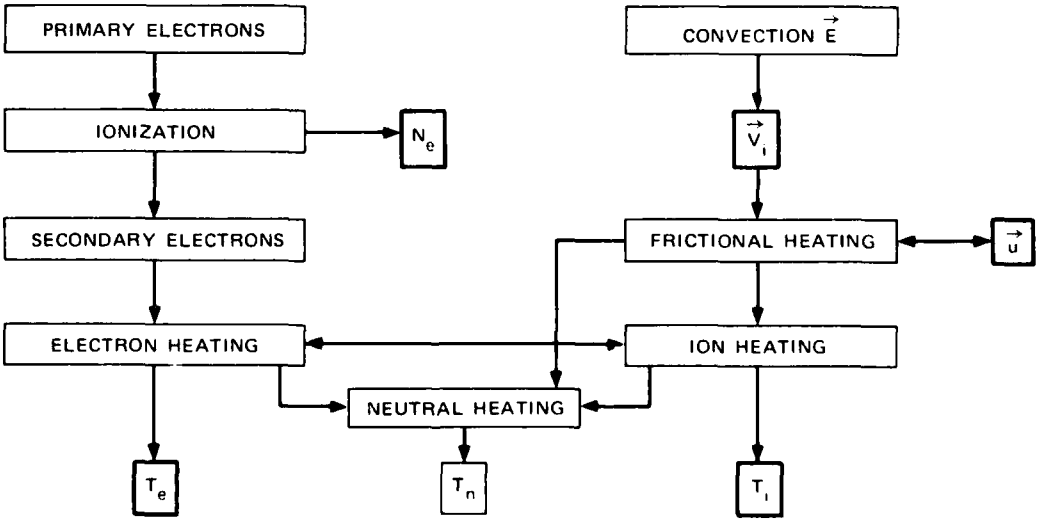

FIGURE 1 AURORAL BLOCK DIAGRAM (adapted from Rees, 1975)

A. Particle Precipitation and Electron Temperature

On the left side of the auroral diagram we indicate the heating process due to auroral electrons. A flux of energetic electrons bombards the upper atmosphere, the depth of penetration depending on the electron energy. Most of the energy is deposited between 100- and 120-km altitude. The energetic primary electrons transfer energy through the ionization of the ambient neutral constituents (N_2, O_2, and O). The collision reactions are:

$$N_2 + e \longrightarrow N_2^+ + 2e \qquad (1)$$

$$N_2 + e \longrightarrow N^+ + N + 2e \qquad (2)$$

$$O_2 + e \longrightarrow O_2^+ + 2e \qquad (3)$$

$$O_2 + e \longrightarrow O^+ + O + 2e \qquad (4)$$

$$O + e \longrightarrow O^+ + 2e \qquad (5)$$

In the above ionizing reactions some of the energy from primary electrons goes into the production of excited states of N^+, O^+, N, and O. Enhanced vibrational and rotational levels of N_2^+, O_2, and O_2^+ are also produced. The secondary electrons have energies of tens of electron volts. Much of this energy is lost in inelastic collisions with neutrals and finally the remaining energy is shared with the ambient electrons producing a temperature enhancement.

B. Joule Heating and Ion Temperature

Referring again to Figure 1, the right side indicates the process of heating by electric fields perpendicular to the magnetic field. Magnetospheric-$\vec{E}$ fields are mapped down along magnetic field lines and are consequently applied to the ionosphere. The field produces $\vec{E} \times \vec{B}$ drift of both ions and electrons. As the ions drift through the neutral atmosphere they collide with neutrals and frictional heating (or joule heating) results.

The ion temperature can exceed both the neutral and electron temperatures at ionospheric heights. Temperature enhancements of 2000 K (3 times ambient) have been observed as the result of heating by a 60-mV orthogonal-$\vec{E}$ field.

C. Ionospheric Heating From Nuclear Effects

The radiation from high altitude nuclear explosions will have similar effects on the upper atmosphere as auroral particle precipitation. The UV radiation from the debris kinetic energy and X-ray from prompt and delayed radiation are the primary sources. The prompt and delayed radiation is less important at F-region altitudes. Figure 2 indicates the ionization process and the resultant heating.

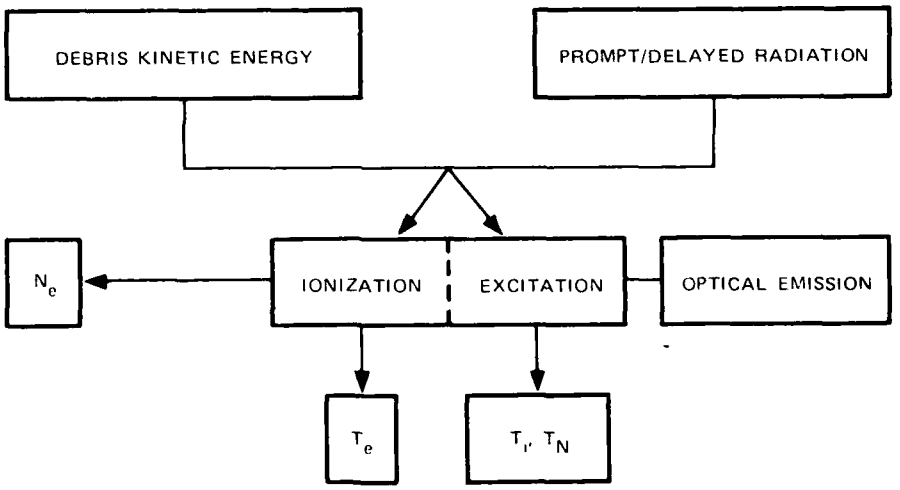

FIGURE 2 IONOSPHERE HEATING FROM NUCLEAR EFFECTS

D. Auroral Zone Ion Composition

In addition to the ionization reactions, the principal auroral ionosphere reactions are as follows:

$$N_2^+ + O \longrightarrow NO^+ + N \qquad (6)$$

$$N_2^+ + O_2 \longrightarrow O_2^+ + N_2 \qquad (7)$$

$$N^+ + O_2 \longrightarrow NO^+ + O \qquad (8)$$

$$N^+ + O_2 \longrightarrow O_2^+ + N \qquad (9)$$

$$O_2^+ + N_2 \longrightarrow NO^+ + NO \qquad (10)$$

$$O_2^+ + N \longrightarrow NO^+ + O \qquad (11)$$

$$O_2^+ + NO \longrightarrow NO^+ + O_2 \qquad (12)$$

$$O^+ + N_2 \longrightarrow NO^+ + N \qquad (13)$$

$$O^+ + O_2 \longrightarrow O_2^+ + O \qquad (14)$$

$$N_2^+ + e \longrightarrow N + N \qquad (15)$$

$$O_2^+ + e \longrightarrow O + O \qquad (16)$$

$$NO^+ + e \longrightarrow N + O \qquad (17)$$

There are also reactions involving excited states-- $O^+(^2D, ^2P)$, $O_2^+(a^4)$ which produce N_2^+ by

$$O^+ (^2D) + N_2 \longrightarrow N_2^+ + O \qquad (18)$$

$$O^+ (^2P) + N_2 \longrightarrow N_2^+ + O \qquad (19)$$

$$O_2^+ (a^4) + N_2 \longrightarrow N_2^+ + O_2. \qquad (20)$$

There are, of course, other reactions, but those listed above are the principal ones.

We have investigated the effects of large $\vec{E}$ fields on the concentrations of NO^+ and O^+ at high latitudes. The measurements indicate that during periods of large $\vec{E}$ fields the dominant F-region ion becomes NO^+ instead of O^+. As a result of this change in ion composition, the F-region ionization rapidly decays because of recombination of the molecular ions.

The following processes contribute to increasing the NO^+ abundance; these are:

- enhanced $[N_2]$
- enhanced ion temperatures
- enhanced N_2 vibrational temperatures.

Enhanced $[N_2]$ arises because, during periods of large joule heating, it is expected that the neutral atmosphere should be heated by ion-neutral collisions. Hays, et al., [1973], have shown that a heated volume element of neutral particles will rise with a vertical velocity which increases with altitude. This expansion will cause an upwelling of N_2 molecules, thereby increasing the number density of N_2 at higher altitudes. In the nuclear case, this phenomena is called "heave." The number density of NO^+ will be enhanced because more N_2 is available to either react with O^+ to form NO^+ (Eq. 13), or be ionized to form N_2^+ (Eq. 1), which in turn reacts with O to form NO^+ (Eq. 6).

The second contributing factor to the enhancement of NO^+ ions is the dependence of certain reaction rate coefficients on ion temperature. The rate coefficient (K_1) for the reaction $O^+ + N_2 \rightarrow NO^+ + N$ from Banks et al., [1974], is

$$K_1 = \begin{cases} 1.2 \times 10^{-12} \left(\frac{300\ K}{T_{eff}}\right) \ cm^3/s & T_{eff} < 750 \\ 8.0 \times 10^{-14} \left(\frac{T_{eff}}{300\ K}\right)^2 \ cm^3/s & T_{eff} > 750 \end{cases},$$

where $T_{eff} = T_n + 0.329\ \vec{E}'^{2}_{\perp}$, and $\vec{E}'_{\perp}$ is the orthogonal $\vec{E}$-field measured in the neutral-wind frame. This is a simplified form assuming $\nu_i/\Omega_i \ll 1$ and B = 0.5 gauss (Polar region). As an example, for an $\vec{E}$ field of 50 mV/m, and T_n = 900 K, T_{eff} will be increased by a factor of 1.9, as compared to T_{eff} for no $\vec{E}$ field. This in turn increases K_1 by a factor of 3.7 . The result should be an enhancement in the number of NO^+ ions. The ions are lost through dissociative recombination. The recombination-rate coefficient decreases with increasing electron temperature [Walls and Dunn, 1974]; consequently, the net result is an increase in the number density of molecular ions.

The third point relative to the production of NO^+ concerns the reaction $O^+ + N_2^* \rightarrow NO^+ + N$, where N_2^* is vibrationally excited N_2. The reaction rates for this reaction are enhanced as compared to $O^+ + N_2$ [Banks et al., 1974]. In the auroral oval, N_2 becomes vibrationally excited through the process

$$e\ (\text{energetic electrons}) + N_2 \rightarrow N_2^* + e \qquad (21)$$

$$N + NO \rightarrow N_2^* + O \qquad (22)$$

$$O\ (^1D) + N_2 \rightarrow N_2^* + O\ (^3P). \qquad (23)$$

All of these processes--i.e., (1) enhanced number density of N_2, (2) enhanced reaction rate coefficients due to elevated T_i, and (3) enhanced reaction coefficients due to vibrational excitation of N_2, act jointly to increase the NO^+ abundance in the F region. The first and second processes are mainly a result of joule heating, and the third process results from electron precipitation.

The nominal lifetime of molecular ions in the presence of moderate electron densities (10^5 el/cm^3) is only a few seconds, whereas the O^+ lifetime is minutes. Consequently, changing the dominant F-region ion to NO^+ results in a depletion of electron density. During the event examined in the study, the critical frequency decreased to about 2.7 MHz from 4.7 MHz.

III MEASURED AURORAL ZONE IONOSPHERIC RESPONSE

The geomagnetic coordinates of the Chatanika incoherent-scatter radar are given in Table 1, and its parameters are given in Table 2.

Table 1

GEOMAGNETIC COORDINATES OF THE CHATANIKA INCOHERENT-SCATTER RADAR

Geographic Coordinates		Dipole Geomagnetic Coordinates		Magnetic Field	
Latitude	Longitude	Latitude	Longitude	Dip Angle	Declination
65.103°N	147.451°W	64.75°N	105.0°W	76.5°	29.0°

Table 2

PARAMETERS OF THE CHATANIKA INCOHERENT-SCATTER RADAR

Operating frequency	1290 MHz
Transmitted peak power	3 to 4 MW
Pulsewidths	60 μs, 160 μs, 320 μs
Effective antenna aperture	180 m^2
Antenna on-axis gain	47.1 dB
Antenna 1/2-power-full-width beamwidth	0.6°
Transmit polarization	Right circular
Receive polarization	Left circular
System noise temperature	110 K
A/D converter sample spacing	10 μs
On-line computer system	XDS 930

The geometrical relationship between Chatanika and the auroral oval for moderate geomagnetic activity is shown in Figure 3. The oval is usually far north of Chatanika at local noon and is often overhead near midnight. The circle (arbitrarily located at 1500 UT) indicates the E-region coverage typical for these experiments.

The Chatanika radar measures the following ionospheric parameters:

(1)	Electron density (N_e)	(backscatter power)
(2)	Ion velocity (V_i)	(doppler shift)
(3)	Temperature ratio (T_e/T_i)	(spectral shape)
(4)	Ion temperature	(spectral shape)

From these measurements other parameters, such as the electric field, currents, and conductivities, are derived.

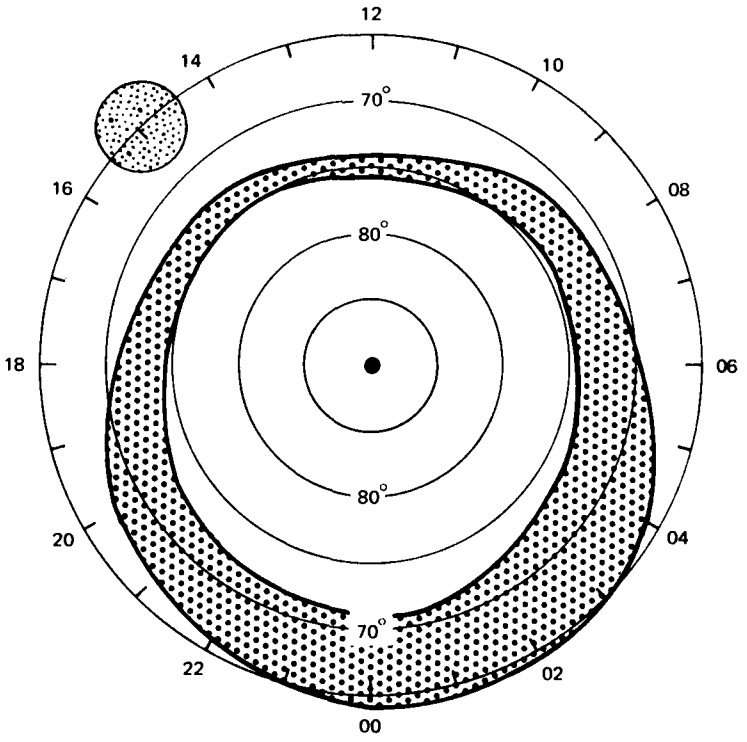

FIGURE 3 CHATANIKA LOCATION (65°N) AND FELDSTEIN'S 1967 AURORAL OVAL. (Source: Feldstein and Starkov, 1967.)

A. Radar Measurements

A representative joule heating event of interest occurred on 13 August 1976. The radar was operated continuously for the entire day. The operating mode was an azimuth scan at a fixed elevation angle of 76.5^{o} (the magnetic dip angle). The time for one antenna scan was about 6 minutes, and the data were integrated over two antenna scans giving 12-minute averages of all the parameters.

The ambient electron density profile is shown in Figure 4. This profile was measured about 45 minutes prior to a large joule heating event. It can be seen that an auroral E-region of about 3×10^5 el/cm^3 and a moderate F region (2×10^5 el/cm^3) existed.

The electric field was computed for the 24-hour period and it shows the characteristic pattern of auroral zone electric fields. In the evening prior to local midnight, the field is directed to the north. Near midnight the field reverses and is directed south during the early morning. The north-south field is plotted in Figure 5. The field becomes quite large at 1400 UT--nearly 60 mV/m. The resulting joule heating is plotted in Figure 6. At 1400 UT the energy input is about 30 ergs/cm^2-s, which is substantial. This is one of the largest joule heating events analyzed in detail and, as will be seen, its effects are considerable.

The electron and ion temperatures at 277 km altitude are shown in Figure 7. At the start of the run, 0000 UT, the ion temperature is fairly constant with a value of 900 K. There is little change in the ion temperature until about 1000 UT, when the joule input begins. There is an obvious enhancement in ion temperature at 1400 UT--the peak of the joule input. The temperature remains elevated even after the joule heat source terminates at 1500 UT, being about 150 K higher than the earlier temperatures. The temperature gradually decreases and it returns to initial conditions by 2300 UT.

The electron temperature shows the effect of the changing Solar-Zenith-Angle (SZA). Initially the temperature is about 2200 K and it gradually decreases with increasing SZA (from 0430 to 0800 UT).

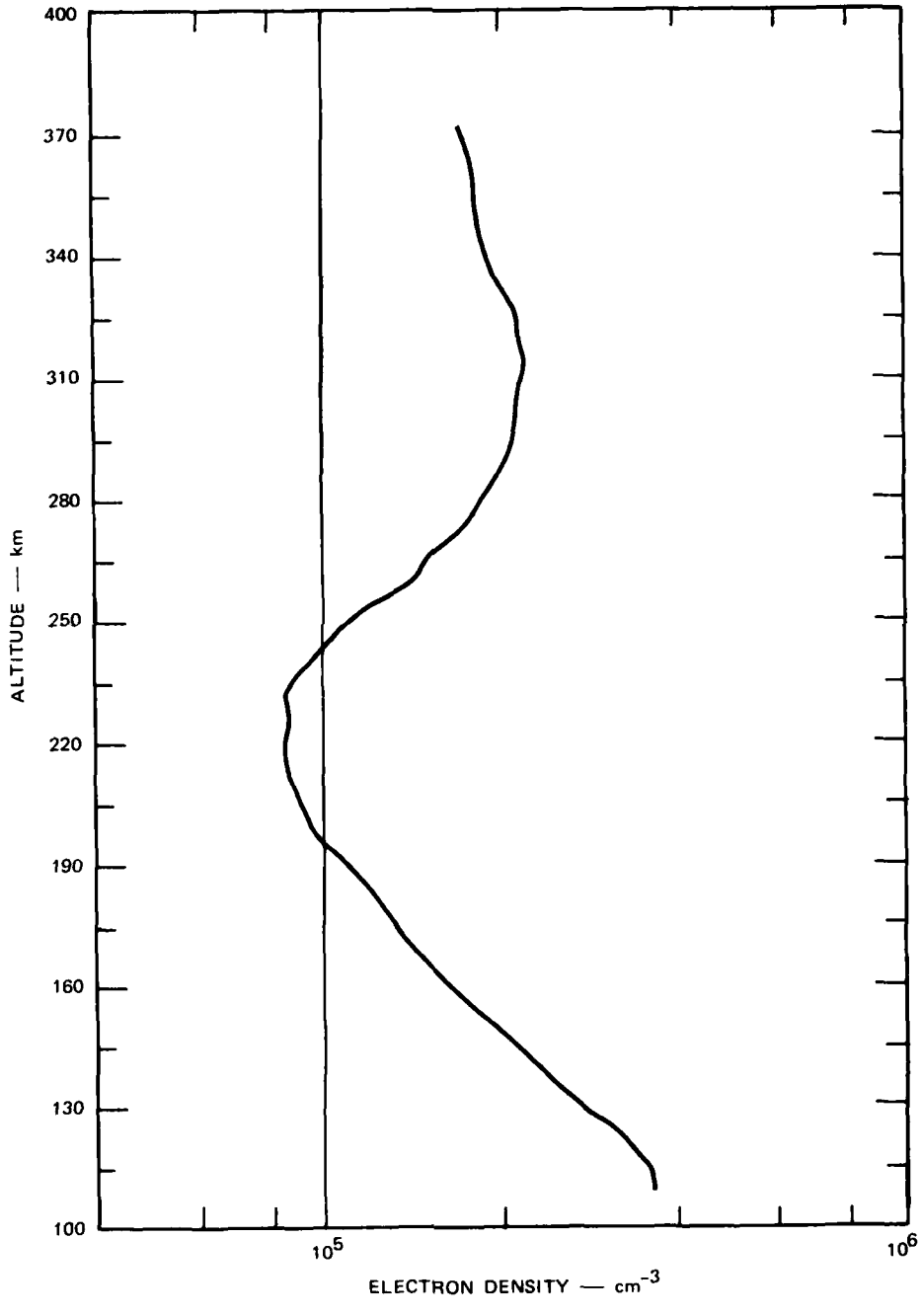

FIGURE 4 AMBIENT ELECTRON DENSITY PROFILE FOR 13 AUGUST 1975

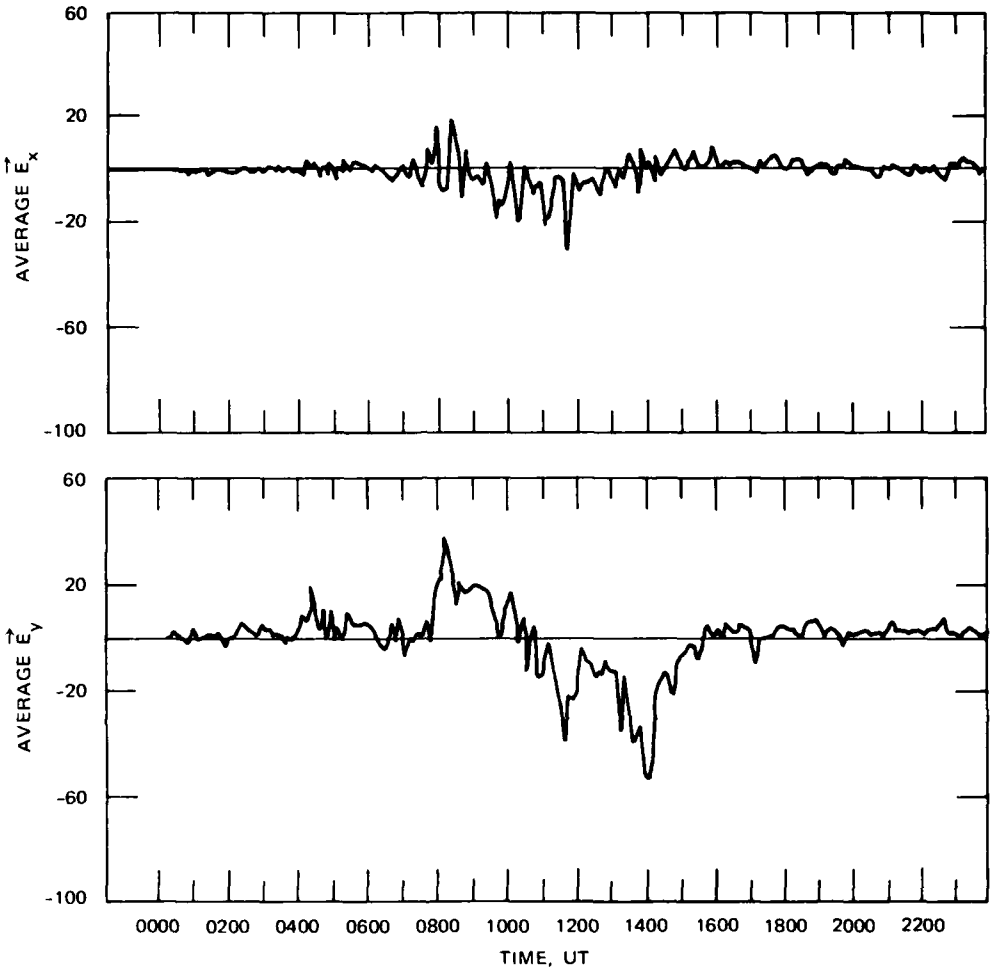

FIGURE 5 AVERAGE ELECTRIC FIELD FOR 13 AUGUST 1975. The Large E_x field (~55 mV/m) at 1400 UT produced substantial joule heating.

The ratio of the number densities of O^+ ions to the total number of ions, $[O^+]/N_e$, is used to describe the ion composition vs. altitude. Figure 8 shows contours of $[O^+]/N_e$ as a function of time for the 13 August event. The transition altitude, the altitude where half the ions are atomic ($[O^+]/N_e = 0.5$), is seen to be near 190 km at the beginning of the observation. However, at 1400 UT, the peak of the heating event, this altitude increases by 50 km--molecular ions dominate below 240 km.

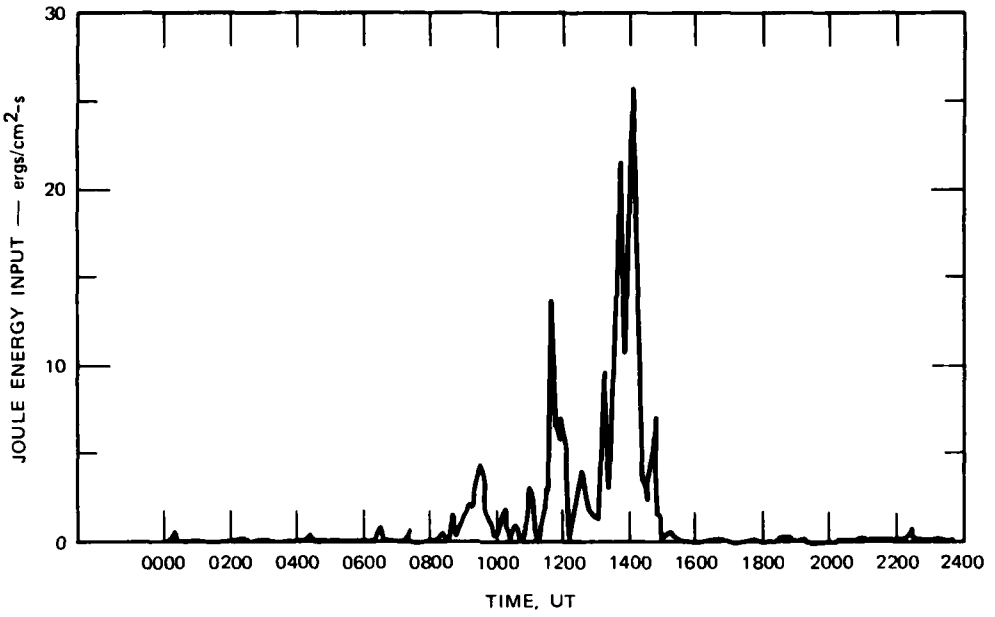

FIGURE 6 HEIGHT-INTEGRATED JOULE HEATING FOR 13 AUGUST 1975

An important consequence of this alteration of ion composition is an immediate decrease of electron density. Molecular ions, O_2^+ and NO^+, recombine much more rapidly than atomic ions and the result is a decay of the lower F region.

Electron density profiles, measured before, during, and after the joule heating event are shown in Figure 9. The F-region depletion can easily be seen. The critical frequency prior to the depletion was about 4.1 MHz. During the heating, the critical frequency dropped to 2.7 MHz and 30 minutes later, it is 3.5 MHz.

To aid in the interpretation of these measurements, we performed a numerical analysis in which we varied parameters such as electron density, production rate, and joule heating rate. The resulting effects on the ion composition agree with the observed data, and are described below.

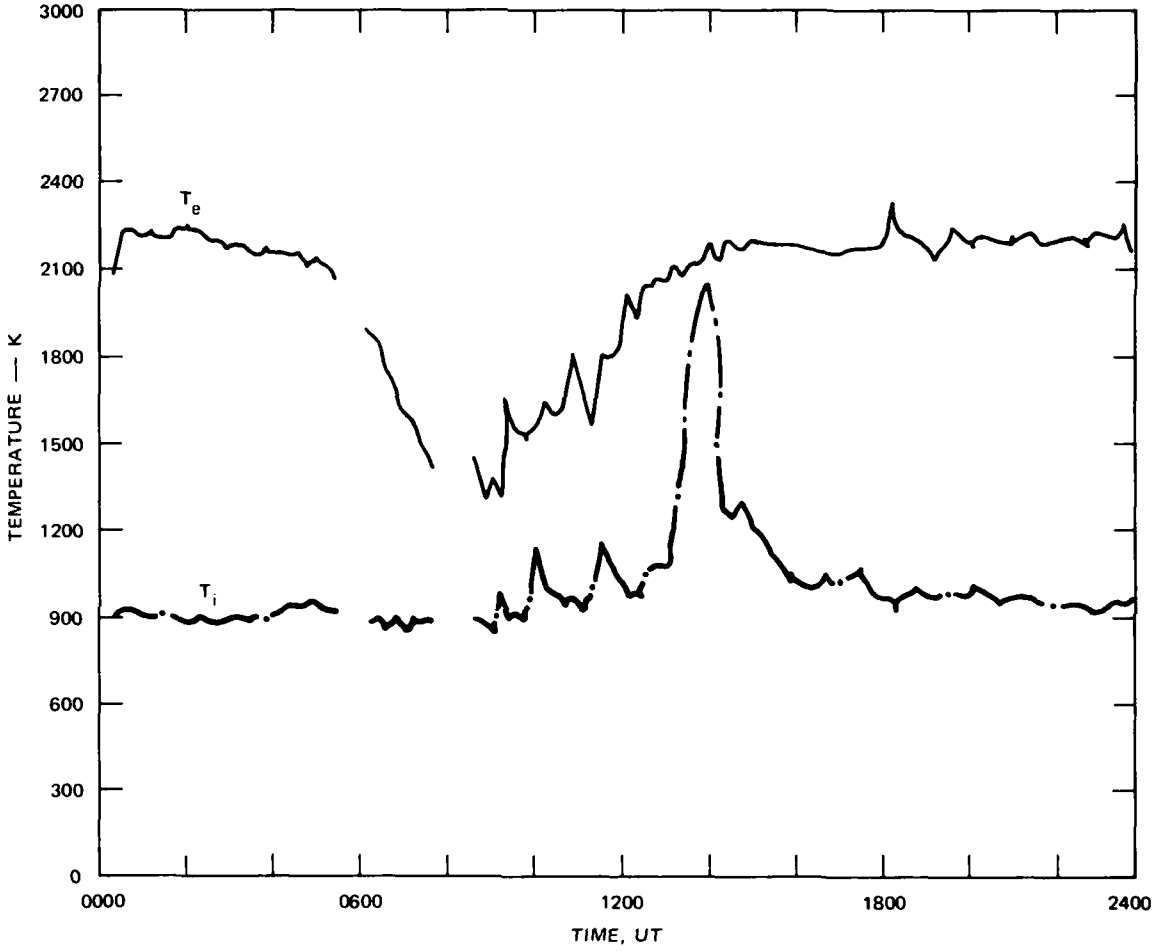

FIGURE 7 ELECTRON AND ION TEMPERATURES AT 277 km FOR 13 AUGUST 1975

B. Numerical Modeling of Transition Altitude Variation

The initial conditions include quiet day and night parameters in order to establish background composition profiles. The change in ion composition can be examined with the aid of an expression derived using the following simplified system of reactions and continuity equations:

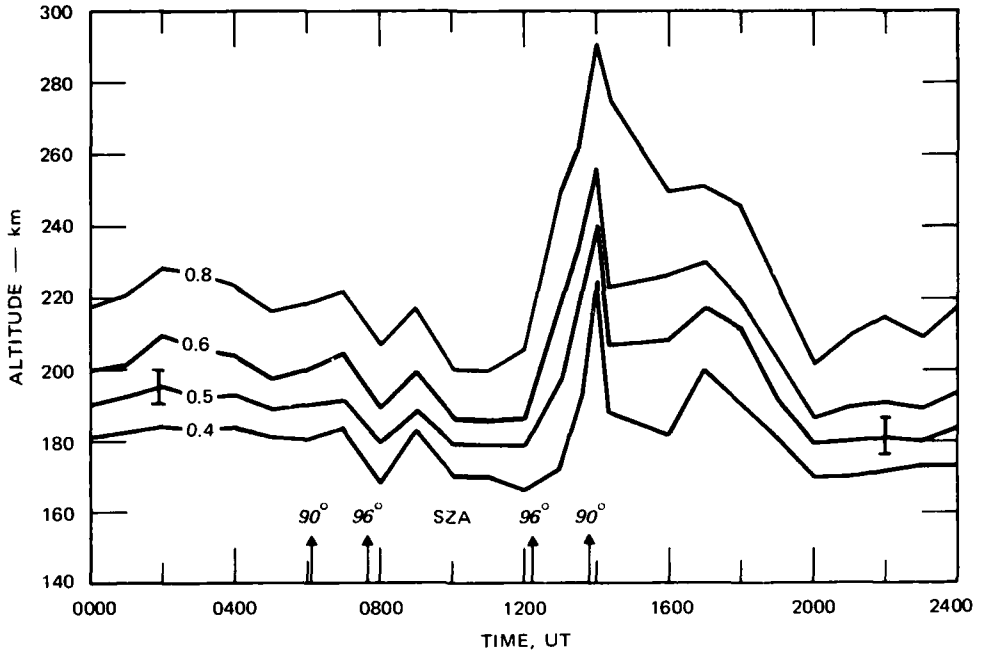

FIGURE 8 ION COMPOSITION CONTOURS FOR 13 AUGUST 1975. At a fixed altitude the ratio of O^+ to total ionization decreased markedly during the joule heating event and increased slowly thereafter. The transition altitude computed during the event is a lower bound with a 5 km uncertainty.

$$O^+ + O_2 \xrightarrow{\gamma_1} O_2^+ + O \qquad \gamma_1 = 2 \times 10^{-11} \left(\frac{300}{T_i}\right)^{1/2}$$

$$O_2^+ + e \xrightarrow{\alpha_1} O + O \qquad \alpha_1 = 2.2 \times 10^{-7} \left(\frac{300}{T_e}\right)$$

$$O^+ + N_2 \xrightarrow{\gamma_2} NO^+ + N \qquad \gamma_2 = 1 \times 10^{-12} \left(\frac{300}{T_i}\right)$$

$$NO^+ + e \xrightarrow{\alpha_2} N + O \qquad \alpha_2 = 4.1 \times 10^{-7} \left(\frac{298}{T_e}\right)$$

$$N_2^+ + O \xrightarrow{\gamma_3} NO^+ + N \qquad \gamma_3 = 1.4 \times 10^{-10}$$

$$N_2^+ + e \xrightarrow{\alpha_3} N + N \qquad \alpha_3 = 2.9 \times 10^{-7} \left(\frac{300}{T_e}\right)^{1/3}$$

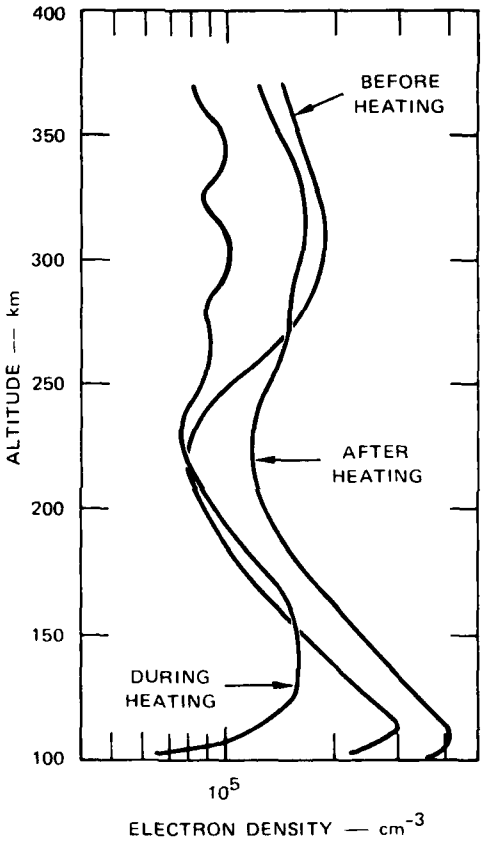

FIGURE 9 ELECTRON DENSITY PROFILES DURING THE JOULE HEATING EVENT ON 13 AUGUST 1975. The F-region density decreases during the event and recovers as the heating subsides.

$$\frac{\partial[O^+]}{\partial t} = q(O^+) - \gamma_1[O_2][O^+] - \gamma_2[N_2][O^+] = 0$$

$$\frac{\partial[NO^+]}{\partial t} = \gamma_2[N_2][O^+] + \gamma_3[N_2^+][O] - \alpha_2[NO^+]N_e = 0$$

$$\frac{\partial[O_2^+]}{\partial t} = q(O_2^+) + \gamma_1[O_2][O^+] - \alpha_1[O_2^+]N_e = 0$$

$$\frac{\partial[N_2^+]}{\partial t} = q(N_2^+) - \gamma_3[N_2^+][O] - \alpha_3[N_2^+]N_e = 0 \quad ,$$

where q(x) is the production rate of species x. If steady state is assumed, the number densities of the various ions are expressed as:

$$[NO^+] = \frac{\gamma_2[N_2][O^+]}{\alpha_2 N_e} + \frac{\gamma_3[N^+][O]}{\alpha_3 N_e}$$

$$[O_2^+] = \frac{q(O_2^+) + \gamma_1[O_2][O^+]}{\alpha_3 N_e}$$

$$[N_2^+] = \frac{q(N_2^+)}{\gamma_3[O] + \alpha_e N_e} \quad .$$

Substitution of the above into the expression for charge neutrality,

$$N_e = [O^+] + [NO^+] + [O^+]$$

and solving for $[O^+]/N_e$, gives

$$\frac{[O^+]}{N_e} = \frac{1}{\frac{\gamma_1[O_2] + \gamma_2[N_e]}{q(O^+)}\left[\frac{\gamma_3[N_2^+][O]}{\alpha_2 N_e} + \frac{q(O_2^+)}{\alpha_1 N_e}\right] + \frac{\gamma_2[N_2]}{\alpha_2 N_e} + \frac{\gamma_1[O_2]}{\alpha_1 N_e} + 1} \quad ,$$

where

$$q(O^+) = \frac{0.56[O]\eta}{1.15[N_2] + 1.5[O_2] + 0.56[O]}$$

$$q(O_2^+) = \frac{[O_2]\eta}{1.15[N_2] + 1.5[O_2] + 0.56[O]}$$

$$[N_2^+] = \frac{q(N_e^+)}{\gamma_3[O] + \alpha_3 N_e}$$

$$= \left[\frac{0.92[N_2]\eta}{1.15[N_2] + 1.5[O_2] + 0.56[O]}\right] / (\gamma_3[O] + \alpha_3 N_e)$$

and η = total ion production rate [Jones and Rees, 1973]. The effects on the transition altitude of varying the atmospheric density, electron density, production rate, and temperature can then be assessed.

1. Quiet Conditions--Diurnal Variation

The model atmosphere used in all cases was taken from Banks and Kockarts for an exospheric temperature of 1000 K, and the ionospheric parameters were obtained from Chatanika radar data. The model atmospheric and ionospheric data are given in Table 3. The calculated composition profiles are shown in Figure 10. The difference in the profiles is most pronounced above 180 km. Above that altitude, the daytime electron density is at least an order of magnitude larger than the nighttime density. The transition altitude increases by about 20 km at night.

Table 3

MODEL ATMOSPHERE AND IONOSPHERIC DATA FOR QUIET DAY AND NIGHT

Quiet Day

Alt (km)	N_e (cm^{-3})	T_i (K)	T_e (K)	$[O_2]$ (cm^{-3})	$[O]$ (cm^{-3})	$[N_2]$ (cm^{-3})
140	7.5E4*	596	650	4.40E9	2.44E10	5.37E10
160	1.0E5	765	1000	1.20E9	1.13E10	1.67E10
180	1.2E5	861	1600	4.43E8	6.45E9	6.88E9
200	1.5E5	916	1800	1.87E8	4.07E9	3.22E9
220	2.0E5	948	2000	8.48E7	2.69E9	1.60E9
240	3.0E5	967	2000	4.00E7	1.83E9	8.26E8
260	2.5E5	979	2000	1.93E7	1.26E9	4.36E8
280	2.45E5	986	2000	9.43E6	8.80E8	2.33E8
300	2.0E5	991	2000	4.67E6	6.20E8	1.26E8

Quiet Night

Alt (km)	N_e (cm^{-3})	T_i (K)	T_e (K)	$[O_2]$ (cm^{-3})	$[O]$ (cm^{-3})	$[N_2]$ (cm^{-3})
140	8.6E4	596	596	4.40E9	2.44E10	5.37E10
160	7.0E4	765	765	1.20E9	1.13E10	1.67E10
180	5.6E4	861	861	4.43E8	6.45E9	6.88E9
200	5.0E4	916	916	1.87E8	4.07E9	3.22E9
220	3.4E4	948	943	8.48E7	2.69E9	1.60E9
240	3.0E4	965	965	4.00E7	1.83E9	8.26E8

*7.5E4 = 7.5×10^4.

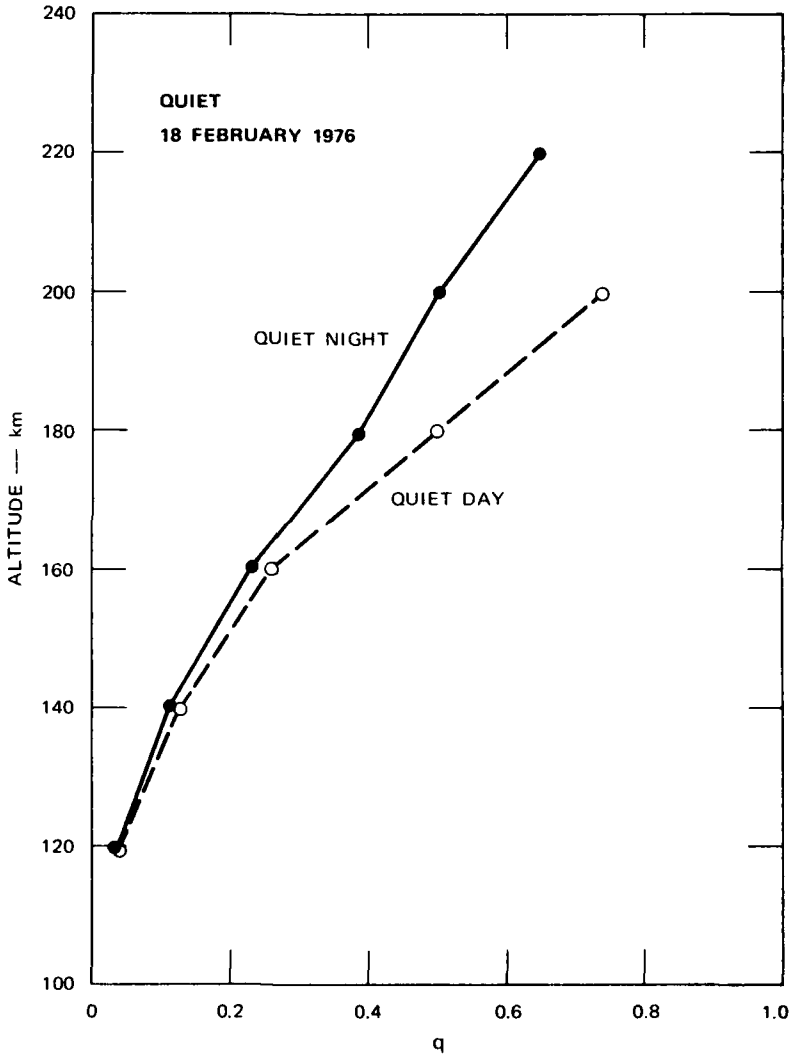

FIGURE 10 MODEL COMPOSITION PROFILES SHOWING DIURNAL VARIATION

2. Active Conditions--Particle Precipitation

The effects of electron precipitation that are considered are enhanced N_e, electron temperature, and vibrational temperature of N_2. The atmospheric and ionospheric parameters are given in Table 4. The first case considered uses temperature and N_e profiles from data taken on 18 February 1976. The particle energy input rate was approximately 20 ergs/cm^2-s. The composition profiles shown in Figure 11 indicate that, relative to the background profile (quiet night), the transition altitude is lower by more than 20 km. In fact, the transition altitude is lower in this case than it was using daytime conditions.

The effects of enhanced vibrational temperatures of N_2 are examined using the above (active night) model. According to Schunk and Banks [1975], the vibrational temperatures during an auroral substorm can be in the range 1400 to 2200 K. These temperatures will increase the N_2 and O^+ reaction-rate coefficient (γ_2) by 1.5 to 3.6 times the ground-state coefficient. Consequently, the composition profiles were recomputed applying those factors to γ_2. The results are shown in Figure 12. There is a substantial increase in the transition altitude for the case when T_v = 2200 K.

Table 4

MODEL ATMOSPHERE AND IONOSPHERIC DATA FOR ACTIVE (AURORA) NIGHT

Alt (km)	N_e (cm^{-3})	T_i (K)	T_e (K)	$[O_2]$ (cm^{-3})	$[O]$ (cm^{-3})	$[N_2]$ (cm^{-3})
140	2.0E5	596	750	4.40E9	2.44E10	5.37E10
160	1.3E5	765	1120	1.20E9	1.13E10	1.67E10
180	1.5E5	861	1300	4.43E8	6.45E9	6.88E9
200	1.8E5	916	1800	1.87E8	4.07E9	3.22E9
220	1.9E5	948	2000	8.48E7	1.83E9	1.60E9

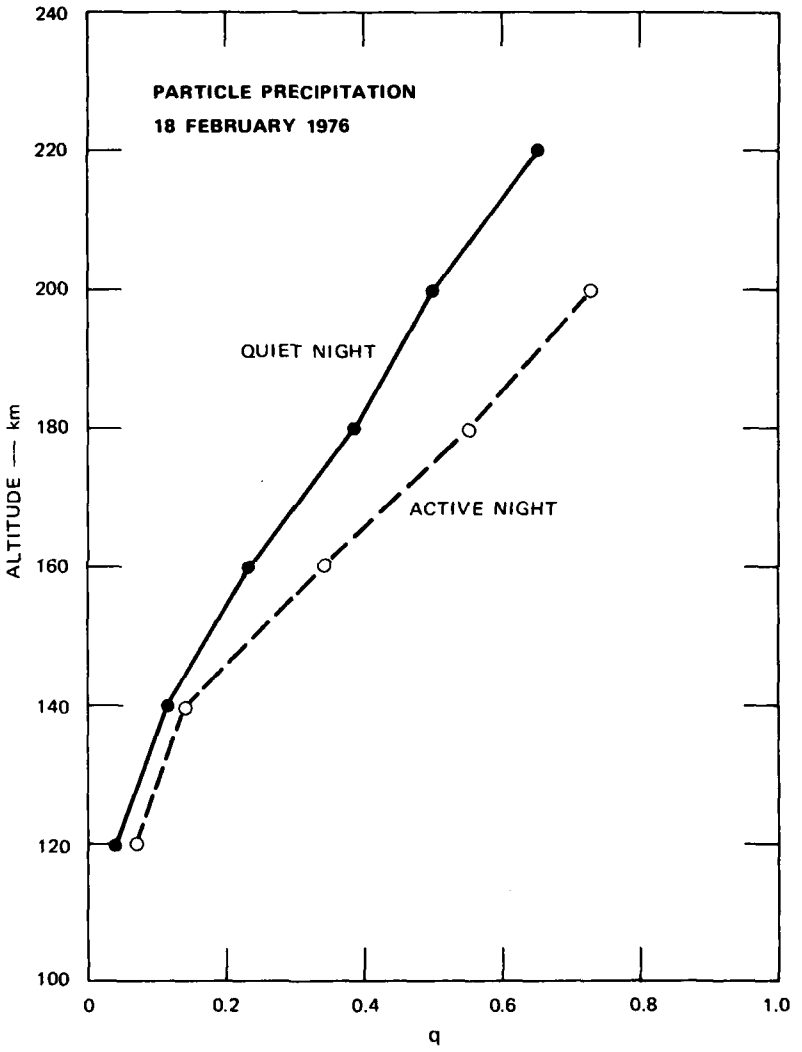

FIGURE 11 MODEL COMPOSITION PROFILES SHOWING THE EFFECTS OF AURORAL IONIZATION

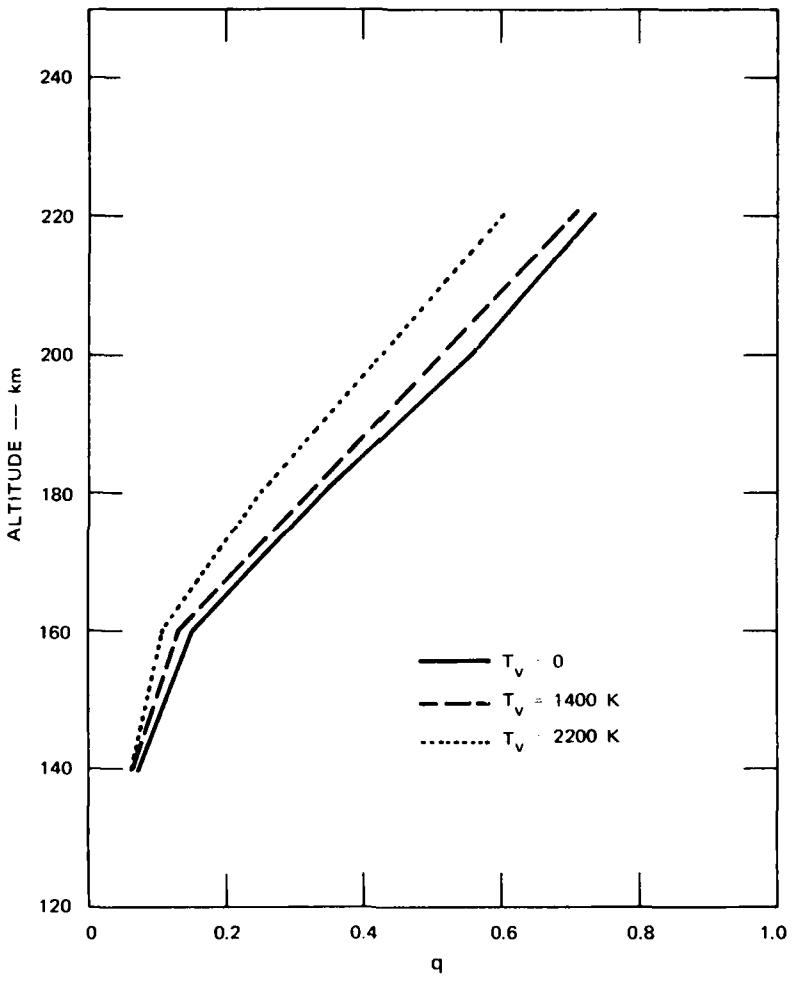

FIGURE 12 COMPOSITION PROFILES SHOWING THE EFFECT OF ENHANCED N_2 VIBRATIONAL TEMPERATURE. The model from Table 4 was used and the reaction-rate coefficient for $N_2 + O^+$ was enhanced.

3. Effect of Joule Heat Input

The atmospheric model and ionospheric data used to evaluate the effect of joule heat are given in Table 5. The ionospheric data--i.e., electron density, and electron/ion temperatures were taked from 13 August 1975 data. The composition profile (Figure 13) corresponding to the active data indicates that more molecular ions exist at all altitudes as compared to the quiet period. The transition altitude increased by 20 km. The active period was characterized by elevated ion temperature and decreased electron density; both factors contribute to the increase of the transition altitude.

Table 5

MODEL ATMOSPHERE AND IONOSPHERIC DATA USED TO EVALUATE THE EFFECT OF JOULE HEAT

Active Day (Joule Heating)

Alt (km)	N_e (cm^{-3})	T_i (K)	T_e (K)	$[O_2]$ (cm^{-3})	$[O]$ (cm^{-3})	$[N_2]$ (cm^{-3})
160	2.0E5	830	965	1.20E9	1.13E10	1.67E10
190	1.2E5	1050	1400	2.85E8	5.08E9	4.66E9
220	1.5E5	1200	2000	8.48E7	2.69E9	1.60E9
276	1.0E5	1800	2000	9.60E6	9.00E8	2.50E8

Quiet Day

Alt (km)	N_e (cm^{-3})	T_i (K)	T_e (K)	$[O_2]$ (cm^{-3})	$[O]$ (cm^{-3})	$[N_2]$ (cm^{-3})
160	2.0E5	765	965	1.20E9	1.13E10	1.67E10
190	2.3E5	1100	1784	2.85E8	5.08E9	4.66E9
220	3.5E5	1600	2000	8.48E7	2.69E9	1.60E9

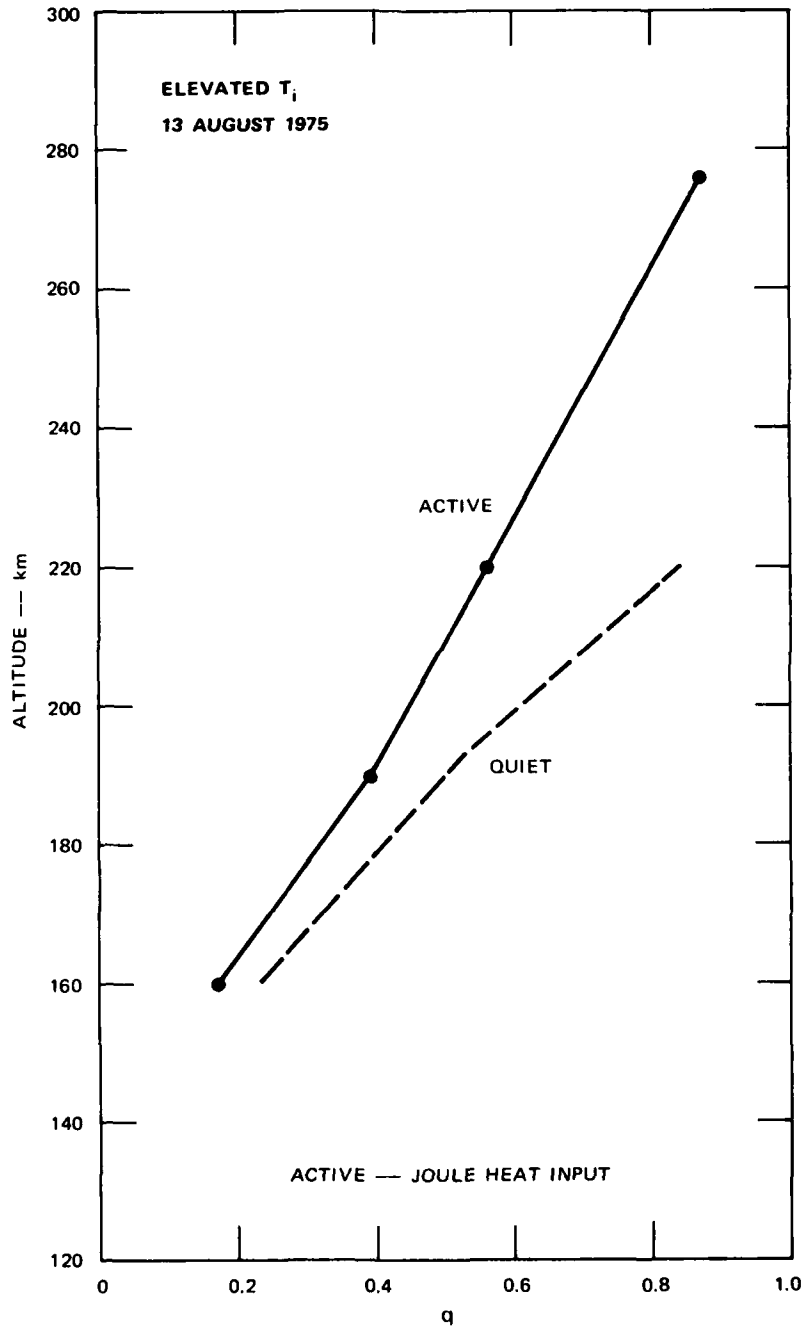

FIGURE 13 COMPOSITION PROFILE CORRESPONDING TO THE JOULE HEAT INPUT COMPARED TO THE QUIET PERIOD

C. Summary of Numerical Modeling

We have just shown that the ion composition at a given altitude changes as a function of the production and loss rates. Factors that contribute to the enhancement of the production rate tend to increase the relative abundance of O^+ ions. These factors are Solar EUV radiation during the day and energetic auroral electron bombardment at night. Both the radar data and the numerical modeling indicate lower transition altitudes during these periods.

Factors that contribute to the enhancement of the loss rate tend to increase the relative abundance of molecular ions. These factors include elevated ion and neutral temperatures, and enhanced vibrational temperatures of N_2 molecules. The ion temperature and the N_2 vibrational temperature determine the rate coefficient and the neutral temperature defines the N_2 number density.

IV CONCLUSIONS

Impulsive ionospheric heating events resulting from auroral energy input have been observed by the Chatanika radar. In some cases, the time--and height--integrated auroral energy deposition is comparable to that expected from a high altitude nuclear event outside the fireball region.

In the auroral event, virtually all ionospheric parameters (electron density, ion, electron and neutral temperatures, and ion and neutral composition) are strongly affected. This would also be the case for extended regions outside a nuclear fireball. The increased temperatures and the resulting atmospheric heave contribute to a change in ion composition such that molecular ions (NO^+, O_2^+) dominate over atomic ions (O^+). Since molecular ions recombine much more rapidly than atomic ions, the net electron density decreases. The region affected by this depletion is larger than the region affected by the fireball and debris.

The nuclear effects codes do not attempt to accurately model this region. Consequently, they do not accurately predict ionospheric effects of nuclear explosions beyond the fireball region. In fact, the ambient atmosphere and ionosphere models are not realistic compared to observed parameters.

The Chatanika radar provides relevant information concerning both the ambient and aurorally disturbed ionosphere. These results can be used to improve the nuclear effects codes so that the much larger region beyond the fireball is more realistically modeled.

REFERENCES

Banks, P. M., R. W. Schunk and W. J. Raitt, "NO^+ and O^+ in the High-Latitude F-Region," Geophys. Res. Letters, Vol. 1, pp. 239-242 (1974).

Feldstein, Y. I., and G. V. Starkov, "Dynamics of Auroral Belt and Polar Geomagnetic Disturbances," Planet. Space Sci., Vol. 15, pp. 209-229 (1967).

Hays, P. B., R. A. Jones, and M. H. Rees, "Auroral Heating and the Composition of the Neutral Atmosphere," Planet. Space Sci., Vol. 21, pp. 559-573 (1973).

Jones, R. A. and M. H. Rees, "Time Dependent Studies of the Aurora--I. Ion Density and Composition," Planet. Space Sci., Vol. 21, pp. 537-557 (1973).

Rees, M. H., "Magnetospheric Substorm Energy Dissipation in the Atmosphere," Planet. Space Sci., Vol. 23, pp. 1589-1596 (1975).

Schunk, R. W., and P. M. Banks, "Auroral N_2 Vibrational Excitation and the Electron Density Trough," Geophys. Res. Letters, Vol. 2, No. 6, pp. 239-242 (1975).

Walls, F. L. and G. H. Dunn, "Measurement of Total Cross Sections for Electron Recombination with NO^+ and O_2^+ using Ion Storage Techniques," J. Geophys. Research, Vol. 79, pp. 1911-1915 (1974).

DISTRIBUTION LIST

DEPARTMENT OF DEFENSE

Assistant Secretary of Defense
Comm., Cmd., Cont. & Intell.
ATTN: Dir. of Intelligence Systems, J. Babcock
ATTN: C3IST&CCS, M. Epstein

Assistant to the Secretary of Defense
Atomic Energy
ATTN: Executive Assistant

Command & Control Technical Center
ATTN: C-312, R. Mason
ATTN: C-650, G. Jones
3 cy ATTN: C-650, W. Heidig

Defense Advanced Rsch. Proj. Agency
ATTN: TIO

Defense Communications Agency
ATTN: Code 101B
ATTN: Code 810, J. Barna
ATTN: Code 205
ATTN: Code 480
ATTN: Code R1033, M. Raffensperger
ATTN: Code 480, F. Dieter

Defense Communications Engineer Center
ATTN: Code R123
ATTN: Code R410, R. Craighill
ATTN: Code R720, J. Worthington
ATTN: Code R410, J. McLean

Defense Intelligence Agency
ATTN: DT-1B
ATTN: HQ-TR, J. Stewart
ATTN: DB, A. Wise
ATTN: DC-7D, W. Wittig
ATTN: DT-5
ATTN: DB-4C, E. O'Farrell

Defense Nuclear Agency
ATTN: STVL
ATTN: DDST
3 cy ATTN: RAAE
4 cy ATTN: TITL

Defense Technical Information Center
12 cy ATTN: DD

Field Command
Defense Nuclear Agency
ATTN: FCPR

Field Command
Defense Nuclear Agency
Livermore Division
ATTN: FCPRL

Interservice Nuclear Weapons School
ATTN: TTV

Joint Chiefs of Staff
ATTN: J-3, WWMCCS Evaluation Office
ATTN: C3S
ATTN: J-37

DEPARTMENT OF DEFENSE (Continued)

Joint Strat. Tgt. Planning Staff
ATTN: JPST, G. Goetz
ATTN: JLTW-2

National Security Agency
ATTN: W-32, O. Bartlett
ATTN: R-52, J. Skillman
ATTN: B-3, F. Leonard

Undersecretary of Defense for Rsch. & Engrg.
ATTN: Strategic & Space Systems (OS)

WWMCCS System Engineering Org.
ATTN: R. Crawford

DEPARTMENT OF THE ARMY

Assistant Chief of Staff for Automation & Comm.
Department of the Army
ATTN: DAAC-ZT, P. Kenny

Atmospheric Sciences Laboratory
U.S. Army Electronics R&D Command
ATTN: DELAS-EO, F. Niles

BMD Systems Command
Department of the Army
2 cy ATTN: BMDSC-HW

Deputy Chief of Staff for Ops. & Plans
Department of the Army
ATTN: DAMO-RQC

Electronics Tech. & Devices Lab.
U.S. Army Electronics R&D Command
ATTN: DELET-ER, H. Bomke

Harry Diamond Laboratories
Department of the Army
ATTN: DELHD-N-RB, R. Williams
ATTN: DELHD-N-P, F. Wimenitz
ATTN: DELHD-I-TL, M. Weiner
ATTN: DELHD-N-P

U.S. Army Comm.-Elec. Engrg. Instal. Agency
ATTN: CCC-CED-CCO, W. Neuendorf
ATTN: CCC-EMEO, W. Nair
ATTN: CCC-EMEO-PED, G. Lane

U.S. Army Communications Command
ATTN: CC-OPS-WR, H. Wilson
ATTN: CC-OPS-W

U.S. Army Communications R&D Command
ATTN: DRDCO-COM-RY, W. Kesselman

U.S. Army Foreign Science & Tech. Ctr.
ATTN: DRXST-SD

U.S. Army Materiel Dev. & Readiness Cmd.
ATTN: DRCLDC, J. Bender

U.S. Army Nuclear & Chemical Agency
ATTN: Library

DEPARTMENT OF THE ARMY (Continued)

U.S. Army Satellite Comm. Agency
ATTN: Document Control

U.S. Army TRADOC Systems Analysis Activity
ATTN: ATAA-TCC, F. Payan, Jr.
ATTN: ATAA-PL
ATTN: ATAA-TDC

DEPARTMENT OF THE NAVY

Joint Cruise Missile Project Office
Department of the Navy
ATTN: JCM-G-70

Naval Air Development Center
ATTN: Code 6091, M. Setz

Naval Air Systems Command
ATTN: PMA 271

Naval Electronic Systems Command
ATTN: PME 117-20
ATTN: PME 117-211, B. Kruger
ATTN: PME 117-2013, G. Burnhart
ATTN: PME 106-13, T. Griffin
ATTN: Code 3101, T. Hughes
ATTN: PME 106-4, S. Kearney
ATTN: Code 501A

Naval Intelligence Support Ctr.
ATTN: NISC-50

Naval Ocean Systems Center
ATTN: Code 532, J. Bickel
ATTN: Code 5322, M. Paulson
3 cy ATTN: Code 5324, W. Moler

Naval Research Laboratory
ATTN: Code 7550, J. Davis
ATTN: Code 6700, T. Coffey
ATTN: Code 6780, S. Ossakow
ATTN: Code 7500, B. Wald

Naval Space Surveillance System
ATTN: J. Burton

Naval Surface Weapons Center
ATTN: F-31

Naval Surface Weapons Center
ATTN: Code F-14, R. Butler

Naval Telecommunications Command
ATTN: Code 341

Office of Naval Research
ATTN: Code 421
ATTN: Code 420

Office of the Chief of Naval Operations
ATTN: OP 604C
ATTN: OP 941D
ATTN: OP 981N

Strategic Systems Project Office
Department of the Navy
ATTN: NSP-2141
ATTN: NSP-2722, F. Wimberly
ATTN: NSP-43

DEPARTMENT OF THE AIR FORCE

Aerospace Defense Command
Department of the Air Force
ATTN: DC, T. Long

Air Force Avionics Laboratory
ATTN: AAD, W. Hunt
ATTN: AAD, A. Johnson

Air Force Geophysics Laboratory
ATTN: OPR-1, J. Ulwick
ATTN: LKB, K. Champion
ATTN: OPR, A. Stair
ATTN: PHI, J. Buchau
ATTN: PHP, J. Aarons
ATTN: PHP, J. Mullen

Air Force Weapons Laboratory, AFSC
ATTN: SUL
ATTN: DYC

Air Logistics Command
Department of the Air Force
ATTN: OO-ALC/MM, R. Blackburn

Assistant Chief of Staff
Intelligence
Department of the Air Force
ATTN: INED

Assistant Chief of Staff
Studies & Analyses
Department of the Air Force
ATTN: AF/SASC, G. Zank
ATTN: AF/SASC, W. Adams

Ballistic Missile Office
Air Force Systems Command
ATTN: MNNH, M. Baran
ATTN: MNNL, S. Kennedy
ATTN: MNNH

Deputy Chief of Staff
Operations Plans and Readiness
Department of the Air Force
ATTN: AFXOKCD
ATTN: AFXOXFD
ATTN: AFXOKS
ATTN: AFXOKT

Deputy Chief of Staff
Research, Development, & Acq.
Department of the Air Force
ATTN: AFRDS
ATTN: AFRDSP
ATTN: AFRDQ
ATTN: AFRDSS

Electronic Systems Division
Department of the Air Force
ATTN: DCKC, J. Clark

Electronic Systems Division
Department of the Air Force
ATTN: XRW, J. Deas

Electronic Systems Division
Department of the Air Force
ATTN: YSEA
ATTN: YSM, J. Kobelski

DEPARTMENT OF THE AIR FORCE (Continued)

Foreign Technology Division
Air Force Systems Command
ATTN: SDEC, A. Oakes
ATTN: NIIS Library
ATTN: TQTD, B. Ballard

Headquarters Space Division
Air Force Systems Command
ATTN: SZJ, L. Doan
ATTN: SZJ, W. Mercer

Rome Air Development Center
Air Force Systems Command
ATTN: TSLD
ATTN: OCS, V. Coyne

Rome Air Development Center
Air Force Systems Command
ATTN: EEP

Strategic Air Command
Department of the Air Force
ATTN: OOKSN
ATTN: XPFS
ATTN: DCXF
ATTN: NRT
ATTN: DCX
ATTN: DCXT, T. Jorgensen
ATTN: DCXT

Headquarters Space Division
Air Force Systems Command
ATTN: SKA, M. Clavin
ATTN: SKA, C. Rightmyer

DEPARTMENT OF ENERGY CONTRACTORS

EG&G, Inc.
Los Alamos Division
ATTN: Document Control for D. Wright
ATTN: Document Control for J. Colvin

Lawrence Livermore Laboratory
ATTN: Document Control for Technical Information Dept. Library

Los Alamos Scientific Laboratory
ATTN: Document Control for P. Keaton
ATTN: Document Control for D. Westervelt
ATTN: Document Control for R. Taschek

Sandia Laboratories
ATTN: Document Control for Org. 1250 W. Brown
ATTN: Document Control for 3141
ATTN: Document Control for Space Project Div.
ATTN: Document Control for D. Thornbrough
ATTN: Document Control for D. Dahlgren

Sandia Laboratories
Livermore Laboratory
ATTN: Document Control for T. Cook
ATTN: Document Control for B. Murphey

OTHER GOVERNMENT AGENCIES

Central Intelligence Agency
ATTN: OSI/PSTD

OTHER GOVERNMENT AGENCIES (Continued)

Department of Commerce
National Bureau of Standards
ATTN: Security Officer for R. Moore

Department of Commerce
National Oceanic & Atmospheric Admin.
Environmental Research Laboratories
ATTN: R. Grubb

Institute for Telecommunications Sciences
National Telecommunications & Info. Admin.
ATTN: D. Crombie
ATTN: L. Berry
ATTN: W. Utlaut

U.S. Coast Guard
Department of Transportation
ATTN: G-DOE-3/TP54, B. Romine

DEPARTMENT OF DEFENSE CONTRACTORS

Aerospace Corp.
ATTN: T. Salmi
ATTN: N. Stockwell
ATTN: R. Slaughter
ATTN V. Josephson
ATTN: F. Morse
ATTN: S. Bower
ATTN: D. Olsen
ATTN: I. Garfunkel

University of Alaska
ATTN: T. Davis

Analytical Systems Engineering Corp.
ATTN: Radio Sciences

Analytical Systems Engineering Corp.
ATTN: Security

Barry Research Communications
ATTN: J. McLaughlin

BDM Corp.
ATTN: T. Neighbors
ATTN: L. Jacobs

Berkeley Research Associates, Inc.
ATTN: J. Workman

Boeing Co.
ATTN: S. Tashird
ATTN: G. Hall
ATTN: D. Murray
ATTN: J. Kenney

University of California at San Diego
ATTN: H. Booker

Charles Stark Draper Lab., Inc.
ATTN: D. Cox
ATTN: J. Gilmore

Computer Sciences Corp.
ATTN: H. Blank

Comsat Labs
ATTN: R. Taur
ATTN: G. Hyde

DEPARTMENT OF DEFENSE CONTRACTORS (Continued)

Cornell University
ATTN: D. Farley, Jr.

Electrospace Systems, Inc.
ATTN: H. Logston

ESL, Inc.
ATTN: J. Marshall
ATTN: J. Roberts
ATTN: C. Prettie

Ford Aerospace & Communications Corp.
ATTN: J. Mattingley

General Electric Co.
ATTN: M. Bortner

General Electric Co.
ATTN: A. Steinmayer
ATTN: C. Zierdt
ATTN: S. Lipson

General Electric Co.
ATTN: F. Reibert

General Electric Company-TEMPO
ATTN: M. Stanton
ATTN: T. Stevens
ATTN: DASIAC
ATTN: W. Knapp
ATTN: D. Chandler

General Electric Tech. Services Co., Inc.
ATTN: G. Millman

General Research Corp.
ATTN: J. Ise, Jr.
ATTN: J. Garbarino

GTE Sylvania, Inc.
ATTN: M. Cross

HSS, Inc.
ATTN: D. Hansen

IBM Corp.
ATTN: F. Ricci

University of Illinois
ATTN: Security Supervisor for K. Yeh

Institute for Defense Analyses
ATTN: E. Bauer
ATTN: J. Aein
ATTN: H. Wolfhard
ATTN: J. Bengston

International Tel. & Telegraph Corp.
ATTN: G. Wetmore
ATTN: Technical Library

JAYCOR
ATTN: S. Goldman

JAYCOR
ATTN: D. Carlos

Kaman Sciences Corp.
ATTN: T. Meagher

DEPARTMENT OF DEFENSE CONTRACTORS (Continued)

Johns Hopkins University
ATTN: J. Newland
ATTN: T. Evans
ATTN: B. Wise
ATTN: P. Komiske
ATTN: Document Librarian
ATTN: T. Potemra

Linkabit Corp.
ATTN: I. Jacobs

Litton Systems, Inc.
ATTN: R. Grasty

Lockheed Missiles & Space Co., Inc.
ATTN: W. Imhof
ATTN: R. Johnson
ATTN: M. Walt

Lockheed Missiles & Space Co., Inc.
ATTN: Dept 60-12
ATTN: D. Churchill

M.I.T. Lincoln Lab
ATTN: L. Loughlin
ATTN: D. Towle

McDonnell Douglas Corp.
ATTN: J. Moule
ATTN: W. Olson
ATTN: N. Harris
ATTN: G. Mroz

Mission Research Corp.
ATTN: R. Hendrick
ATTN: S. Gutsche
ATTN: R. Bogusch
ATTN: F. Fajen
ATTN: D. Sowle

Mitre Corp.
ATTN: B. Adams
ATTN: A. Kymmel
ATTN: C. Callahan
ATTN: G. Harding

Mitre Corp.
ATTN: W. Hall
ATTN: W. Foster
ATTN: M. Horrocks

Pacific-Sierra Research Corp.
ATTN: E. Field, Jr.

Photometrics, Inc.
ATTN: I. Kofsky

Physical Dynamics, Inc.
ATTN: E. Fremouw

R & D Associates
ATTN: B. Yoon
ATTN: L. Delaney

Rand Corp.
ATTN: C. Crain
ATTN: E. Bedrozian

DEPARTMENT OF DEFENSE CONTRACTORS (Continued)

R & D Associates
ATTN: W. Karzas
ATTN: M. Gantsweg
ATTN: R. Turco
ATTN: C. Greifinger
ATTN: H. Ory
ATTN: W. Wright, Jr.
ATTN: C. MacDonald
ATTN: B. Gabbard
ATTN: R. Lelevier
ATTN: F. Gilmore

Riverside Research Institute
ATTN: V. Trapani

Rockwell International Corp.
ATTN: J. Kristof

Santa Fe Corp.
ATTN: E. Ortlieb

Science Applications, Inc.
ATTN: L. Linson
ATTN: C. Smith
ATTN: D. Hamlin
ATTN: J. McDougall
ATTN: D. Sachs
ATTN: E. Straker

Science Applications, Inc.
ATTN: D. Divis

Science Applications, Inc.
ATTN: SZ

DEPARTMENT OF DEFENSE CONTRACTORS (Continued)

SRI International
ATTN: W. Jaye
ATTN: A. Burns
ATTN: G. Smith
ATTN: G. Price
ATTN: M. Baron
ATTN: D. Neilson
ATTN: C. Rino
ATTN: R. Leadabrand
ATTN: R. Livingston
ATTN: W. Chesnut
3 cy ATTN: J. Kelly

Teledyne Brown Engineering
ATTN: R. Deliberis

Tri-Com, Inc.
ATTN: D. Murray

TRW Defense & Space Sys. Group
ATTN: S. Altschuler
ATTN: R. Plebuch
ATTN: D. Dee

Utah State University
ATTN: K. Baker
ATTN: L. Jensen

Visidyne, Inc.
ATTN: J. Carpenter